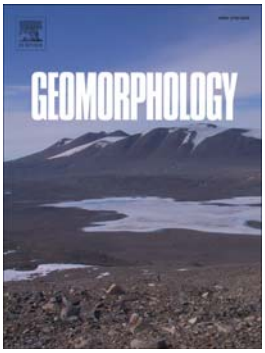

Recent spatial and temporal variations in debris cover on Patagonian glaciers

Neil F. Glasser, Thomas O. Holt, Zachary D. Evans, Bethan J. Davies, Mauri Pelto, Stephan Harrison

PII: S0169-555X(16)30316-6
DOI: doi: 10.1016/j.geomorph.2016.07.036
Reference: GEOMOR 5709

To appear in: *Geomorphology*

Received date: 13 May 2016
Revised date: 19 July 2016
Accepted date: 27 July 2016

Please cite this article as: Glasser, Neil F., Holt, Thomas O., Evans, Zachary D., Davies, Bethan J., Pelto, Mauri, Harrison, Stephan, Recent spatial and temporal variations in debris cover on Patagonian glaciers, *Geomorphology* (2016), doi: 10.1016/j.geomorph.2016.07.036

Recent spatial and temporal variations in debris cover on Patagonian glaciers

Neil F. Glasser[a*], Thomas O. Holt[a], Zachary D. Evans[a], Bethan J. Davies[b], Mauri Pelto[c], Stephan Harrison[d]

[a]Department of Geography and Earth Sciences, Aberystwyth University, Wales, SY23 3DB, UK

[b]Department of Geography, Royal Holloway, University of London, Egham, Surrey, TW20 0EX, UK

[c]Environmental Science, Nichols College, Dudley, MA, USA

[d]College of Life and Environmental Sciences, University of Exeter, Cornwall Campus, Penryn, TR10 9EZ, UK

[*]Corresponding author. Tel.: +44 1970 622785; E-mail: nfg@aber.ac.uk

Abstract

Supraglacial debris cover is an important component of glacier mass balance, especially in areas characterised by widespread glacier recession. Mapping of the spatial and temporal changes in debris cover on the surface of the receding outlet glaciers of the temperate North Patagonian Icefield (NPI) in southern South America between 1987 and 2015 shows that the total amount of debris cover has increased over time, from 168 km^2 in 1987 to 307 km^2 in 2015. The number of debris-covered glaciers increased from 24 in 1987, to 31 in 2001 to 32 out of 43 studied glaciers in 2015. The proportion of debris-covered area has also increased, from 4.1% in 1987 to 7.9% in 2015, with the largest proportional increases occurring east of the ice divide (where 15.2% of the glacier ice is now debris covered). Over this time, the total area of the NPI decreased from 4133 to 3887 km^2. The area occupied by proglacial and ice-proximal lakes also increased from 112 to 198 km^2. Between 1987 and 2015, the terminal environment of many of the outlet glaciers of the NPI changed from land-terminating to lake-calving, and these glaciers are now receding into terminal lakes. The change in the area of debris-covered ice is influenced by the loss of ice at debris-covered termini and by an increase in debris cover at higher elevations. The glaciers of the NPI remain highly dynamic as they recede and are therefore behaving very differently to high-elevation glaciers, such as those of the Himalaya where debris cover leads to glacier stagnation at the termini.

Keywords: glacier; debris; Patagonia

1. Introduction

Global climate change is driving the behavior of mountain glaciers worldwide (Kaab et al., 2012; Marzeion et al., 2014). While most of these glaciers are undergoing terminus recession or rapid surface lowering, many glaciers in high mountain regions of the world are also accumulating surface debris as the surrounding valley sides and lateral moraines discharge rock and sediment. While our understanding of the ways in which debris-covered glaciers evolve is incomplete, surface debris clearly affects the rate and pattern of glacier melting. As a result, a better understanding of these processes is important if we are to assess the response of mountain glaciers to present and future climate change. Here we use 28 years of observational data to map the spatial and temporal changes in debris cover on the outlet glaciers of the North Patagonian Icefield (NPI), one of the largest mid-latitude ice masses, and relate these to changes in glacier recession and terminal environment.

1.1. Debris-covered glaciers

Debris-covered glaciers have large areas of their ablation area (and occasionally part of their accumulation area) covered by a layer of rock debris, including dust, ash, and sediment of various sizes (Cogley et al., 2011). This supraglacial debris originates from a variety of different sources, including rock avalanches and rockfalls from surrounding valley sides (Benn et al., 2012; Deline and Kirkbride, 2009; Hewitt, 2009; Shugar et al., 2012). Supraglacial debris can also accumulate where englacial and subglacial debris is elevated to the ice surface in the ablation area (Goodsell et al., 2005, Kirkbride and Deline, 2013; Jennings et al., 2014). Supraglacial debris becomes progressively concentrated at glacier termini and margins in areas where the ice-surface velocity, and therefore debris transport rates, are low (Hambrey et al., 2008).

Supraglacial debris cover is an important component of glacier mass balance because it acts as a barrier between the ice surface and the atmosphere. Ablation rates beneath a debris cover are lower than on clean-ice glaciers because the debris layer protects the underlying ice from solar radiation and thermally insulates the underlying ice (Nakawo and Takahashi 1982; Pelto, 2000). Supraglacial debris cover therefore strongly influences surface energy balance and ablation (Kirkbride, 2000; Jansson and Fredin, 2002). The nature of this relationship depends critically on the debris thickness (Østrem, 1959). The presence of supraglacial debris initially causes *increased* ablation because rock debris has a lower albedo than ice (Nakawo and Rana, 1999). The debris thickness at which maximum ablation occurs is referred to as the effective thickness and is typically between 0.01 and 0.05 m (Mattson, 2000). Above this effective thickness, ablation *decreases* with increasing debris thickness (Mihalcea et al., 2008; Brock et al., 2010). The presence of a supraglacial debris layer and variations in its thickness therefore affects how a glacier responds to climatic change.

Glaciers with extensively debris-covered ablation areas tend to lose mass by surface lowering rather than terminus recession (Bolch et al., 2008).

Debris-covered and clean-ice glaciers react differently to externally imposed changes in climate (Scherler et al., 2011; Pellicciotti et al., 2015). Using a numerical model, Rowan et al. (2015) demonstrated that supraglacial debris slows down the response of a glacier to atmospheric warming and causes surface lowering of the glacier *in situ* rather than recession at the terminus, concealing the magnitude of mass loss when compared with estimates based on glacierized area alone. Much of this research on debris-covered glaciers has concentrated on glaciers in the Hindu-Kush Himalaya (e.g., Collier et al., 2015), central Andes (e.g., Janke et al., 2015), and New Zealand (e.g., Benn et al., 2004). Comparatively little has been written about the large outlet glaciers of the temperate icefields in Patagonia. This omission is surprising; the outlet glaciers of the Patagonian Icefields are amongst the most dynamic on Earth, with high accumulation rates, high ablation rates, and rapid rates of terminus recession. They also display a wide range of terminating environments including marine and lacustrine calving glaciers, and they form the Earth's largest mid-latitude temperate ice masses. As a result, their future evolution and the interplay between Southern Hemisphere regional climate and glacier dynamics are of considerable interest. Consequently, in this paper we consider the spatial and temporal changes in debris cover over the last ~28 years between 1987 and 2015 on the dynamically receding outlet glaciers of the temperate North Patagonian Icefield (NPI) and the relationship between glacier recession, supraglacial debris, and changes in terminal environment.

1.2 Study area: The North Patagonian Icefield (NPI)

Understanding the past, present, and future dynamics of the glaciers of the Northern Patagonia Icefield (NPI; Fig. 1; 47.0°S, 73.5°W) and the Southern Patagonia Icefield (SPI; 50.0°S, 73.5°W) is important because they are the largest temperate ice masses in the Southern Hemisphere (Aniya et al., 1996) and their behaviour reflects the operation of important oceanic and atmospheric circulation. In 2001, the NPI had an overall area of 3953 km^2 (Rivera et al., 2007). It is drained by 28 main outlet glaciers (Aniya, 1988). The two largest outlet glaciers are Glaciars San Quintin and San Rafael which, with areas of ~760 km^2, are almost equal in size (Aniya, 1988). Next in size are Glaciars Steffen and Colonia, both of which have similar areas of ~450 km^2. Collectively, these four glaciers occupy ~2416 km^2, equivalent to 57% of the total area of the NPI (Aniya, 1988; Davies and Glasser, 2012). The outlet glaciers of the NPI are either land-terminating or terminate in proglacial lakes (e.g., Glaciars San Quintín, Nef, Leones, Reicher, and Gualas). The exception is Glaciar San Rafael, the closest tidewater glacier to the Equator, which calves into a tidal laguna of the Pacific Ocean.

The outlet glaciers of the NPI and SPI are receding rapidly (Davies and Glasser, 2012; White and Copland, 2015) and thinning (Chen et al., 2007; Willis et al., 2012). Davies and Glasser (2012) calculated that the glacierized area for the NPI between the Little Ice Age (LIA; A.D. ~1870) and 2011 reduced by 660 km^2, equivalent to a 14.2% overall reduction over that time period. Mouginot and Rignot (2015) compiled a near-complete map of ice velocity of the NPI from multiple synthetic aperture radar and optical data collected between 1984 and 2014. These data show that the largest outlet glaciers remain dynamic during recession. The fastest outlet glacier of the NPI, Glaciar San Rafael, flows at 7.6 km/y and the second largest glacier, Glaciar San Quintìn, flows about 1.1 km/y in its narrowest section.

Geologically, the NPI sits on top of homogeneous units, corresponding to calc-alkaline plutons (granite, granodiorites, and tonalites of Lower Cretaceous age) of the Patagonian Batolith (Sernageomin, 2003; Ghiglione et al., 2016a) related to Jurassic-Cenozoic subduction of the Pacific plates underneath South America (Ghiglione et al., 2016b). Toward the west, Triassic basement rocks composed of low grade meta-turbidites, schists, and phyllites outcrop (Sernageomin, 2003). Toward the eastern flank, basement rock belonging to the Eastern Andes Metamorphic complex and the Río Lácteo Formation outcrop. Even farther east, and toward the fold- and thrust-belt and foothills, are small Miocene plutons, the El Quemado Jurassic volcanic complex, and Early Cretaceous to Miocene sediments of the northern Austral basin (Ghiglione et al., 2016a).

Tectonically, the NPI is located at the latitude of the Chile Triple Junction, where subduction of the active Chile ridge produces active strike-slip deformation concentrated along the Liquiñi-Ofqui fault zone, a dextral strike-slip fault of approximately N-S orientation (Georgieva et al., 2016; Ghiglione et al., 2016a, 2016b). Recent geomorphic, thermochronological, and structural data document neotectonic activity along a number of faults along both flanks of the NPI (Georgieva et al., 2016).

Climatologically, this area of Patagonia is characterised by extreme precipitation and climate gradients with a particularly strong west to east decline in precipitation across the NPI (Lenaerts et al., 2014). Glacier equilibrium line altitudes (ELAs) on the NPI range from 870 to 1529 masl, and ELAs are lower on the west side of the icefield (Barcaza et al., 2009). Glacier recession in this area of Patagonia has been attributed to regional changes in temperature and precipitation, with regional atmospheric warming most commonly cited as the causal factor (Rosenblüth et al., 1995; Ibarzabal et al., 1996; Carrasco et al., 2002; Rasmussen et al., 2007; Aravena and Luckman, 2009).

The Patagonian Icefields make a significant contribution to global sea-level rise (Rignot et al., 2003; Rivera et al., 2007; Glasser et al., 2011). Aniya (1999) calculated the contribution of the NPI to sea-level rise between 1945 and 1996 as 0.0105 ± 0.0043 mm/y based upon direct measurements of ice elevation and areal changes experienced mainly in the ablation

area. Rignot et al. (2003) found an ice-loss contribution to sea-level rise for the NPI of 0.008 ± 0.001 mm/y by comparison of digital elevation models (DEMs) for the period 1975–2000. Rivera et al. (2007) estimated a sea-level rise contribution from the NPI of 0.013 ± 0.006 mm/y by DEM comparison and satellite imagery analysis for the period 1979 to 2001. Willis et al. (2012) added speed and surface melt conditions to DEM analysis to find a sea-level rise of 0.009 ± 0.0002 mm/y between 2000 and 2011 for the NPI. Over longer timescales, Glasser et al. (2011) calculated ice losses for the NPI and SPI since the Little Ice Age using field determination of trimlines and terminal moraines. They compared former and contemporary glacier extents to calculate a lower sea-level contribution of 0.0018 ± 0.0004 mm/y between A.D. 1870 and 2004, but then a marked acceleration of ice-loss rates after that date.

2. Methods and data sources

Mapping of glaciers and debris cover was based on visual interpretation of repeat cloud-free satellite images covering the NPI from 1987 (Landsat TM, 80-m resolution), 2001 (Landsat ETM+, 15-30 m resolution) and 2015 (Landsat OLI, 15-30 m resolution; sSee Table 1 and Fig. 2). Glacier outlines from 1987 and 2001 are derived from the data set generated by Davies and Glasser (2012), available from the GLIMS database (Pfeffer et al., 2014). Glacier outlines for 2015 used the 2011 outlines generated by Davies and Glasser (2012), manually edited to reflect glacier extent in 2015. Ice divides followed Davies and Glasser (2012) and remained unchanged throughout the study period.

Supraglacial debris has the same spectral characteristics as lateral and terminal moraines and glaciofluvial deposits and bedrock outside the glacier margin, and therefore cannot be detected using multispectral classification alone (Paul et al., 2004). We therefore applied manual delineation of debris-covered glaciers using on-screen digitizing, evaluated by three individual users to limit uncertainty. Ice-contact lakes at the margins of the glaciers of the NPI were also digitized. All information was stored in ArcGIS.

To assess temporal change, we calculated the area of debris cover for individual glaciers at three time intervals: in 1987, 2001, and 2015 (Table 1). This equates to a time difference of 5064 days (13.9 years) between mapping in 2001 and 2015 and 5144 days (14.1 years) between 1987 and 2001 (Table 2). The entire study period covers the difference between 1987 and 2015 (28 years). On Glaciar San Quintin only, partial cloud cover means that the time elapsed between mapping periods in 2001 and 2014 is 13.7 years (Table 3). We present absolute (km^2), relative (%), and annual (% a^{-1}) rates of change in this paper, using these time periods to calculate annual rates of change. Comparing relative (% a^{-1}) rates of change means that glaciers of different sizes can be easily compared.

To assess spatial change, we also calculated debris cover by elevation band. One-hundred-meter elevation bands were derived from the Advanced Spaceborne Thermal Emission and

Reflection Radiometer (ASTER) Global Digital Elevation Model Version 2 (GDEM V2) (http://asterweb.jpl.nasa.gov/gdem.asp). We used these elevation bands to intersect our digitized debris-covered areas for 1987, 2001, and 2015, with the total area per elevation band summed. We recognize that this does not account for any extensive thinning over this time period, but it does provide us with a reference point from which we can assess change in debris cover. Nunataks were excluded from calculations of glacier area (cf. Rignot and Mouginot, 2015, who included nunataks in their calculations of glacier area). Glacier characteristics such as minimum, maximum, and median elevation and mean slope were derived from the ASTER GDEM V2 and were automatically calculated in the GIS. We use mean slope because the minimum/maximum slope is very susceptible to steep cells near glacier boundaries. Velocities for individual outlet glaciers were derived from Mouginot and Rignot (2015).

The Transient Snow Line (TSL) near the end of the ablation season can be identified using aerial photographs or satellite imagery (Hall et al., 1989; Mernild et al., 2013). In this study, the latest observable Landsat image from the melt season in March and April were used. The date of the latest image therefore varies from year to year. Images were obtained using the software package U.S. Geological Survey Globalization Viewer for the period 2013-2016 (using path/row 232/92 and 232/93 for the NPI); 2014-2016 images are from Landsat 8 OLI and 2013 from Landsat 7. All images are false colour RGB composites, bands 3, 4, and 5. The satellite images were georeferenced in ArcMap 9.3 using five topographically unique reference points. The TSL was manually digitized for each scene. The image spatial resolution of 30 m and the Ground Control point registration error of $\pm$48 m combined with mean surface slopes of 0.05–0.15 m m^{-1}, yields an estimated error of ±10 m in TSL elevations.

3. Results

3.1 Glacier characteristics

We calculated glacier area, and supraglacial debris cover and determined the characteristics of proglacial lakes for 43 glaciers of the NPI in 1987, 2001, and 2015. In 2015, the extent of the NPI was 3980.5 km^2 (Table 3). Just two glaciers account for a large part of this area: Glaciar San Quintin and Glaciar San Rafael cover 771.4 and 731.5 km^2 each, respectively. The smallest glacier in the study region is just 1.4 km^2 (Fig. 2).

In 2015, the total area of debris cover was 306.6 km^2, or 7.9% of the area. Average glacier slope ranged from 10.3° to 33.2°, with an average glacier slope over the entire NPI of 21.5°. The percentage of glaciers covered by debris in 2015 ranged from 0% to 43.8%, with the average being 9.5%.

The variation in the absolute and proportional area of glaciers that is debris-covered is high, with considerable spatial variations between glaciers. There is little relationship between debris cover and glacier mean slope, maximum velocity, and glacier area (Table 4). There is a positive correlation (r^2 of 0.56) between absolute glacier area and debris cover (in km^2), but smaller glaciers do not necessarily have a higher proportion (%) of debris cover (no correlation between glacier area and % debris cover). Larger glaciers are associated with larger proglacial lakes.

Glaciers east of the ice divide had up to 44% debris cover, while the glacier with the highest debris cover west of the ice divide is Gualas (14.1%). The average proportion of debris-covered area is 5 ± 2.2% west of the divide and 12.6 ± 5.8% east of the divide (95% confidence interval). A Student's *t*-test further indicated that the individual percentage of glacier debris cover is statistically different east and west of the ice divide (*t* stat 2.52 > *t* crit 1.69), indicating that on average glaciers have a higher proportion of debris cover east of the ice divide. A spatial analysis further reveals that all of the glaciers with a significant proportion of debris cover are on the eastern and northern outlet glaciers of the NPI. The large outlet glaciers on the western NPI have a low proportion of their ice surface covered by debris (Fig 3).

3.2 Overall area changes of the NPI

Glacier area (excluding nunataks) decreased in each time period, from 4133.1 to 3890.5 km^2 in 2015 (Table 5). Glaciers east and west of the ice divide shrank over this time period. The total amount of glacierized area lost is much greater on the west of the icefield (-93.2 km^2 west of the ice divide; -4.8 km^2 east of the ice divide). This equates to a total change of 242.6 km^2 (5.9% of the 1987 area). Almost all glaciers receded, though there was one advance (Glacier ID 74; 1.2 km^2 1987 to 2015). The largest areal losses were from Glaciar San Quintin (-52.7 km^2), Glaciar Steffen (-34.4 km^2), and the Acodado, HPN-3 and HPN-2 systems (-20.6 km^2). These three glaciers alone accounted for 44% of all ice surface area lost on the NPI.

The total overall annual rate of recession has increased, from -0.17% a^{-1} in the period 1987 to 2001 to -0.26% a^{-1} in the period 2001 to 2015. There seems little consistent difference in annual rates of recession (% a^{-1}) east and west of the ice divide, though the larger western glaciers have lost far more absolute area. Annual rates of recession have increased east of the ice divide, but have not changed over the study period west of the ice divide. A Student's *t*-test indicated that rates of recession east and west of the ice divide in the period 1987-2015 are not statistically significant at the 95% confidence level (*t*-stat 0.22 < *t* crit 1.7). There is no statistically significant difference in % annual rates of recession east and west of the ice divide. However, the overall rate of recession has changed significantly between 1987-2001 and 2001-2015 (*t* stat 3.85 > *t* crit 1.67), demonstrating that, across all glaciers of the NPI, the annual rate of recession accelerated after 2001. The fastest rates of

recession from 2001 to2015 was in small glaciers east of the ice divide with no clear relationship between proportion of debris-covered area and annual rates of recession (Fig 3).

3.3 Overall lake area changes of the NPI

Twenty-six glaciers of the NPI had proglacial lakes in 2015, covering 197.7 km^2. Total cumulative lake area was calculated in each time interval for each glacier. Of the 26 glaciers with proglacial lakes, 10 <2 km^2 cumulative lake area (Fig. 2). The largest cumulative lake areas are in front of Glaciar San Quintin (54.6 km^2), Leones (22.8 km^2), and Steffen (20.6 km^2). Loriaux and Casassa (2013) examined the expansion of lakes of the NPI from 1945 to 2011 and concluded that lake area expanded 65%, or 66 km^2, in that time period. The increase in the number of lakes caused an increase in the recession of the glaciers terminating in them because of mass loss through calving.

From 1987 to 2015, the number of glaciers with proglacial lakes increased from 23 to 26, and proglacial lake extent increased from 111.9 to 197.7 km^2, as the lakes have increased in size and flooded overdeepened basins following glacier recession (Table 6). The largest increases are west of the ice divide, where larger glaciers with larger absolute recession (in km^2) have receded further, resulting in the development of larger lakes. The largest lake area increases were identified in front of Glaciar San Quintin (+35.5 km^2), Glaciar Steffen (+8.5 km^2), and the Acodado, HPN3 and HPN2 systems (+8.3 km^2). Figure 6 shows the example of Glaciar Fiero, where the ice-contact lake expanded between 2001 and 2015.

3.4 Overall debris-covered ice area changes of the NPI

Change in supraglacial debris cover is summarised in Table 7. The number of debris-covered glaciers increased from 24 in 1987, to 31 in 2001, and to 32 out of 43 studied glaciers in 2015. The absolute area of debris-covered ice also increased from 168.5 km^2 in 1987, to 228.6 km^2 in 2001, and to 306.6 km^2 in 2015. This equates to a total increase in the proportion of debris-covered glacier surface area from 4.1% in 1987, to 5.7% in 2001, and to 7.9% in 2015. The largest increase in the proportion of debris-covered area was east of the ice divide, where 15.2% of glacier ice is now debris-covered (Table 7).

Glaciar Steffen, Glaciar San Quintin, Glaciar Colonia, Glaciar Grosse, and Glaciar Exploradores each have more than 20 km^2 of debris cover in 2015 (Fig. 7A). Of the individual outlet glaciers, Glaciar San Rafael (+10.7 km^2), Glaciar Colonia (+9.4 km^2), Glaciar Exploradores (+5.5 km^2), and Glaciar Gualas (+4.6 km^2) show the greatest increases in debris-covered area (Fig. 7B). New material was added to the glacier surface by rockfall

events from the surrounding valley walls on Glaciar Grosse, Glaciar Pissis, and Glaciar Leones (Fig. 8). Existing ice-surface debris was transported and redistributed down-ice by glacier flow on Glaciar Colonia and Glaciar Pared Norte (Fig. 9). Three glaciers showed a small reduction in their debris-covered area: Grosse (-7.1 km^2), Verde (-0.6 km^2), and Arco (-0.1 km^2). These losses in debris-covered area are largely because of glacier recession. For example, in 1987 Grosse Glacier ended on a proglacial outwash plain, with little evidence of recent recession and only a few small supraglacial lakes near the margin. By 2015 the glacier had receded 2.4 km with the commensurate growth of a proglacial terminus lake. The lower 4 km of the glacier appears relatively stagnant and is poised to be lost as recession continues. On Verde Glacier, the 1-km retreat in 28 years is substantial for a glacier that is only 5 km long. The lowest 300 m of the glacier is undergoing a transition from debris-covered ice to an ice-cored moraine and no longer represents active glacier ice.

Although there is no clear statistical correlation between glacier maximum velocity and percentage of debris-covered area (Table 4), Fig. 3C demonstrates how the fastest flowing glaciers generally have very little debris cover, and that debris-covered glaciers, which are largely east of the ice divide, tend to be smaller and have slower flow rates. Recent rockfalls, mudslides, and landslides have been a significant contributor to new debris-covered areas (Fig. 8). For example, a large rockfall deposit appeared on the surface of Leones Glacier ~3 km above its terminus between February 2014 and January 2015, extending about 2 km across the glacier (Fig. 10).

4. Discussion

4.1 Relationship between debris cover and annual rates of recession

Debris-covered glaciers tend to recede more slowly than debris-free glaciers because the supraglacial debris slows down the response of a glacier to atmospheric warming and causes surface lowering of the glacier *in situ* rather than recession at the terminus (Rowan et al., 2015). A logical hypothesis is a negative relationship between *proportion* (%) of debris-covered area and annual rates of recession (% a^{-1}). We note that the largest acceleration in annual rates of recession is east of the ice divide. We also note that the largest increase in glacier debris-covered area is also east of the ice divide; the proportion of debris-covered area is higher east of the ice divide (both average percentage and total percentage debris-covered area). Glaciers with a larger debris-covered area are more likely to have experienced a greater amount of glacier recession (in km^2; (r^2 of 0.57; Table 8; Fig. 2). This is probably because larger glaciers are more likely to have more debris cover (glacier area and debris-covered area in km^2 are correlated; Table 4). However, the proportion of debris-covered area (%) is not correlated with rates of recession from 1987 to 2015 (r^2 of 0.02).

Larger glaciers, which tend to have a greater debris-covered surface area (km^2), are therefore losing more area in general. However, we find no clear relationship between proportion of debris-covered area and percentage change in glacier area per annum. Rather, the greatest control on the *total amount* of surface area lost (in km^2) is glacier size, with larger glaciers losing the most ice-covered area. The percentage change in glacier area seems to be controlled by other factors and variables, with the fastest rates of recession in small glaciers east of the ice divide (Fig. 3B).

4.2 Changes in the Transient Snow Line (TSL) and Equilibrium Line Altitude (ELA)

An increase in debris-covered area is related to an increase in exposed glacier ice by a rising Transient Snow Line (TSL). The TSL is the location of the transition from snow cover to bare glacier ice at a particular time during the ablation season (Østrem, 1975), whereas the Equilibrium Line Altitude (ELA) is the altitude of the snow line at the end of the ablation season. To test this hypothesis, the TSL was identified for the 11 glaciers of the NPI near the end of the ablation season using satellite imagery (Table 9). In recent years the ELA has been rising, and the highest observed TSL in the period 2013-2016 averaged 1215 m. Comparison of the highest observed TSL in a year with data for the 1979-2003 ELA presented by Barcaza et al. (2009) indicated a rise of 103 m. This is a minimum value for the ELA rise. The rise in snowline therefore also partly explains the change in debris-covered area simply because, as the TSL rises, more bare ice and debris are exposed.

4.3 Relationship between hypsometry and debris cover

To investigate further the spatial patterns of debris cover and change, we looked at the distribution of debris cover with elevation in 1987, 2001, and 2015 (Fig. 11A) and how its overall distribution has changed over time between 1987 and 2015 (Fig. 11B). In 1987, there was >20 km^2 of debris-covered ice in the 0-100 m elevation band, and this has reduced rapidly up to 2015 (<3 km^2;Fig. 11A). Since 1987, the area of debris-covered ice has greatly expanded at elevations above the 500-m elevation band in concert with the rise in the TSL (Fig. 11B). Ice area loss has also been greatest at lowest elevations (<100 masl) where glaciers are calving into the sea (e.g., Glaciar San Rafael) and into proglacial lakes (e.g., Glaciar San Quintin, Glaciar Steffen, and the Acodado, HPN-3 and HPN-2 systems). As more ice is lost at lower elevations (<100 masl), we see a commensurate increase in lake area and a loss of debris-covered ice area (Fig. 12; Table 10).

4.4 Glacier lake growth

Our new mapping shows ice-marginal lake areas around the periphery of the NPI of 112 km^2 in 1987, 150 km^2 in 2001, and 198 km^2 in 2015. Loriaux and Casassa (2013) also compiled a glacial lake inventory for the periphery of the NPI and measured a total glacial lake area of 102 km^2 in 1945, rising to 168 km^2 in 2011. Our lake area calculations therefore confirm the findings of Loriaux and Casassa (2013) that ice-marginal and moraine-dammed lakes are

increasing in area as the glaciers of the NPI recede. An increasing volume of water is therefore being stored in these lakes, potentially mitigating some of the effects of increased ablation on the NPI to its global sea-level contribution.

4.5 Glacier velocity and debris cover

The flow velocity of the largest outlet glacier of the NPI, Glaciar San Rafael, has been measured at 7.6 km/y or 21 m/d (Willis et al., 2012; Mouginot and Rignot, 2015). The second largest glacier, San Quintìn, is comparable in size to Glaciar San Rafael but terminates in a proglacial lake and reaches its maximum velocity about 29 km from the ice front, at about 1.1 km/y, in the narrowest section of the terminal valley and close to the ELA (Rivera et al., 2007). In 1993 the glacier terminus was advancing into vegetated ground (Winchester and Harrison, 1996), but since then its terminus has been undergoing steady recession with decay of its piedmont lobe (Davies and Glasser, 2012). Mouginot and Rignot (2015) observed high flow rates, >100 m/y, over more than 90% of the lengths of Glaciars San Rafael and San Quintin, indicating a rapid transfer of mass from the source of these glaciers to their termini. These two glaciers are therefore more or less free of surface debris. The third largest outlet glacier of the NPI, Glaciar Steffen, shares a common catchment with HPN-2 and HPN-3, and debris cover here has increased since 2001.

Large rockfalls, mudflows, and debris flows from high mountain slopes constitute a strong paraglacial depositional response to glacier recession and thinning (Shroder et al., 2000). In combination with the transfer of sediment from subglacial locations along shear planes, paraglacial sedimentation is assumed to be the main contributor to supraglacial debris cover in mid-latitude high mountain chains such as New Zealand (Reznichenko et al., 2011) and Morocco (Hughes et al., 2014). Large rockfalls from mountain slopes also contribute debris to glacier surfaces in Patagonia (Winchester and Harrison, 1997; Harrison et al., 2006; Glasser et al., 2009). However, high rates of vegetation colonization of valley sides exposed by glacier downwasting, especially to the west of the ice divide, means that slopes that might produce large amounts of paraglacial debris become rapidly stable within a decade or two of ice recession (Harrison and Winchester, 1997).

The glaciers described here differ from debris-covered glaciers in other high mountain settings. For instance, many Himalayan debris-covered glaciers such as those in Nepal are characterised by low surface velocities leading to surface lowering in their mid-sections and terminus stagnation. Large supraglacial lakes impounded by terminal moraines at the terminus can coalesce to develop the potential to produce Glacial Lake Outburst Floods (GLOFs; Richardson and Reynolds, 2000). Conversely, the debris-covered glaciers we have described here in Patagonia are much more dynamic with higher contemporary ice fluxes and velocities, even as they undergo significant terminus recession. Thus they do not form

the long, debris-covered tongues and moraine-dammed lakes that typify Himalayan glaciers. Further work is required to determine how the behavior of the temperate Patagonian glaciers described here relates to those in other areas, such as Southeast Alaska, which are similar to Patagonia in terms of climate (Pelto et al., 2013).

5. Conclusions

Using satellite images from three different time periods (1987, 2001, and 2015), we have presented the first complete picture of the spatial and temporal changes in debris cover over the last 28 years on the dynamically receding outlet glaciers of the temperate North Patagonian Icefield (NPI). We have related these changes in debris cover to rates of glacier recession, changes in the Transient Snow Line (TSL), glacier velocity, and changes in terminal environment such as proglacial lake growth.

The number of debris-covered glaciers on the NPI increased from 24 in 1987, to 31 in 2001, to 32 out of 43 studied glaciers in 2015. The total amount of debris cover also increased in each time period, from 168.5 km^2 in 1987 to 306.6 km^2 in 2015. The proportion of debris-covered area has also increased, from 4.1% in 1987 to 7.9% in 2015, with the largest proportional increases occurring east of the ice divide (where 15.2% of ice is now debris covered).

Glacier area has shrunk rapidly over this time period, with annual rates of recession increasing from -0.17 % a^{-1} from 1987 to 2001 to -0.26 % a^{-1} from 2001 to 2015. The greatest increase in rates of recession has occurred east of the ice divide, with annual rates of recession reaching 0.37 % a^{-1} from 2001 to 2015. Glacier surface area loss has been greatest at low elevations, near glacier termini. The smaller, debris-free glaciers east of the ice divide are receding fastest, but we find no statistically significant correlation between proportion of debris-covered area and annual rates of glacier recession. We observe a corresponding increase in proglacial lake area over the study period.

The glaciers of the NPI have high mass balance and rapid ice-flow rates that combine to ensure that these glaciers remain dynamic, even during recession. These dynamic temperate glaciers in Patagonia show very different recent geomorphological behavior to other glaciers accumulating surface debris in areas such as the Himalayas.

Acknowledgements

ZE gratefully acknowledges receipt of a 2015 Walter Idris Jones Summer Bursary at Aberystwyth University, during which time most of the ice-debris mapping was carried out. Matias Ghiglione provided useful background geological context.

References

Aniya, M. 1988. Glacier inventory of the Northern Patagonia Icefield, Chile, and variations 1944/45 to 1985/86. *Arctic and Alpine Research* 20, 179-187.

Aniya, M. 1999. Recent glacier variations of the Hielos Patagónicos, South America, and their contribution to sea-level change. *Arctic, Antarctic, and Alpine Research*, 31 (2), 165–173.

Aniya, M., Sato, H., Namse, R., Skvarca, P., Casassa, G., 1996: The use of satellite and airborne imagery to inventory outlet glaciers of the Southern Patagonia Icefield. *Photogrammetric Engineering and Remote Sensing*, 62: 1361–1369.

Aravena, J.-C., Luckman B.H 2009. Spatio-temporal rainfall patterns in Southern South America. *International Journal of Climatology*, 29, 2106–2212.

Barcaza, G., Aniya, M., Matsumoto, T., Aoki, T. 2009. Satellite-derived equilibrium lines in Northern Patagonia Icefield, Chile, and their implications to glacier variations. *Arctic, Antarctic, and Alpine Research*, 41, 174–182.

Benn, D.I., Kirkbride, M.P. Owen, L.A., V. Brazier. 2004. Glaciated valley landsystems. In Evans, D.J.A., ed. *Glacial Landsystems*. London, Edward Arnold, 372–406.

Benn, D. I., Bolch, T., Hands, K., Gulley, J., Luckman, A., Nicholson, L. I., Quincey, D., Thompson, S., Toumi, R., Wiseman, S. 2012. Response of debris-covered glaciers in the Mount Everest region to recent warming, and implications for outburst flood hazards. *Earth Science Reviews,* 114, 156-174.

Bolch, T., Buchroithner, M., Pieczonka, T., Kunert, A. 2008. Planimetric and volumetric glacier changes in the Khumbu Himal, Nepal, since 1962 using Corona, Landsat TM and ASTER data. *Journal of Glaciology* 54: 592–600. DOI: 10.3189/002214308786570782

Brock, B.W., Mihalcea, C., Kirkbride, M.P., Diolaiuti, G., Cutler, M.E.J., Smiraglia, C. 2010. Meteorology and surface energy fluxes in the 2005–2007 ablation seasons at the Miage debris-covered glacier, Mont Blanc Massif, Italian Alps. *Journal of Geophysical Research: Atmospheres* 115: 112–128. DOI: 10.1029/2009JD013224

Carrasco, J., Casassa, G., Rivera A. 2002. Meteorological and climatological aspects of the Southern Patagonia Icefield IN: G. Casassa, F. Sepulveda, R. Sinclair (Eds.), *The Patagonian Icefields. A Unique Natural Laboratory for Environmental and Climate Change Studies*, Kluwer Academic/Plenum Publishers, New York, pp. 29–65

Chen, J. L., Wilson, C. R., Tapley, B. D., Blankenship, D. D., Ivins E. R. 2007. Patagonia Icefield melting observed by Gravity Recovery and Climate Experiment (GRACE), *Geophysical Research Letters 34*, L22501, doi:10.1029/2007GL031871.

Cogley, J. G., Hock, R., Rasmussen, L. A., Arendt, A. A., Bauder, A., Braithwaite, R. J., Jansson, P., Kaser, G., Moller, M., Nicholson, L., Zemp, M. 2011. Glossary of Glacier Mass Balance and Related Terms. *IHP-VII Technical Documents in Hydrology,* 86.

Collier, E., Maussion, F., Nicholson, L.I., Mölg, T., Immerzeel, W. W., Bush, A. B. G. 2015. Impact of debris cover on glacier ablation and atmosphere-glacier feedbacks in the Karakoram. *The Cryosphere*, 9, 1617-1632.

Davies, B.J., Glasser, N.F. 2012. Accelerating shrinkage of Patagonian glaciers from the Little Ice Age (~ AD 1870) to 2011. *Journal of Glaciology* 58, 1063-1084. doi: 10.3189/2012JoG12J026.

Deline, P., Kirkbride, M. P. 2009. Rock avalanches on a glacier and morainic complex in Haut Val Ferret (Mont Blanc Massif, Italy). *Geomorphology,* 103, 80-92.

Georgieva, V., Malnick, D., Schildgen, T.F., Ehlers, T.A., Lagabrielle, Y., Enkelmann, E., Strecker, M.R. 2016. Tectonic control on rock uplift, exhumation and topography above an oceanic-ridge collision – Southern Patagonian Andes (47^{o}S), Chile. *Tectonics* doi: 10.1002/2016TC004120

Ghiglione, M.C. Ramos, V. Cuitiño, J. Barberón, V. (2016a). Growth of the Southern Patagonian Andes (46 -53°S) and their relation to subduction processes. In "*Growth of the Southern Andes*" Edited by A. Folguera; M. Naipauer, L. Sagripanty, M.C. Ghiglione, Orts, D and Giambiagi, LB. Springer Earth System Sciences, 201-240.

Ghiglione, M., Sue, C., Ramos, M.E., Tobal, J.E., Gallardo, R.E. (2016b). The relation between Neogene denudation of the Southernmost Andes and sedimentation in the offshore Argentine and Malvinas basins during the opening of the Drake Passage. In: Ghiglione, M.C. (ed) *Geodynamic Evolution of the Southernmost Andes*: Springer Earth System Sciences, 109-135.

Glasser N.F., Harrison, S., Jansson, K. 2009. Topographic controls on glacier sediment-landform associations around the temperate North Patagonian Icefield. *Quaternary Science Reviews* 28, 2817–2832.

Glasser, N.F., Harrison, S., Jansson, K.N., Anderson, K., Cowley, A. 2011. Global sea-level contribution from the Patagonian Icefields since the Little Ice Age maximum. *Nature Geoscience* 4, 303-307. DOI: 10.1038/ngeo1122.

Goodsell, B., Hambrey, M. J., Glasser, N. F. 2005. Debris transport in a temperate valley glacier: Haut Glacier d'Arolla, Valais, Switzerland. *Journal of Glaciology,* 51, 139-146.

Hall D. K., Chang A. T. C., Foster J. L., Benson C. S., Kovalick W. M. 1989. Comparison of in situ and Landsat derived reflectance of Alaskan glaciers. *Remote Sensing of the Environment* 28, 23–31.

Hambrey, M. J., Quincey, D. J., Glasser, N. F., Reynolds, J. M., Richardson, S. J., Clemmens, S. 2008. Sedimentological, geomorphological and dynamic context of debris-mantled glaciers, Mount Everest (Sagarmatha) region, Nepal. *Quaternary Science Reviews,* 27, 2361-2389.

Harrison, S., Winchester, V. 1997. Age and nature of paraglacial debris cones along the margins of the San Rafael glacier, Chilean Patagonia. *The Holocene* 7, 481-487.

Harrison, S., Glasser, N.F., Winchester, V., Haresign, E., Warren, C.R., Jansson, K.N. 2006. A glacial lake outburst flood associated with recent mountain glacier retreat, Patagonian Andes. *The Holocene*, 16, 611-620.

Hewitt, K. 2009. Rock avalanches that travel onto glaciers and related developments, Karakoram Himalaya, Inner Asia. *Geomorphology,* 103, 66-79.

Hughes, P.D., Fink, D., Fletcher, W.J., Hannah, G. 2014. Catastrophic rock avalanches in a glaciated valley of the High Atlas, Morocco: ^{10}Be exposure ages reveal a 4.5 ka seismic event. *Geological Society of America Bulletin* 126, 1093-1104.

Ibarzabal, T., Hoffmann, J., Naruse R., 1996. Recent climate changes in southern Patagonia. *Bulletin of Glaciological Research*, 14, 29–36.

Janke, J.R., Bellisario, A.C., Ferrando, F.A. 2015. Classification of debris-covered glaciers and rock glaciers in the Andes of central Chile. *Geomorphology*, 241, 98-121.

Jansson, P., Fredin, O. 2002. Ice sheet growth under dirty conditions: implications of debris cover for early glaciation advances. *Quaternary International* 95-96: 35–42. DOI: 10.1016/S1040-6182(02)00025-3

Jennings, S. J. A., Hambrey, M. J., Glasser, N. F. 2014. Ice flow-unit influence on glacier structure, debris entrainment and transport. *Earth Surface Processes and Landforms,* 39, 1279-1292.

Kääb A., Berthier, E., Nuth, C., Gardelle, J., Arnaud, Y. 2012. Contrasting patterns of early twenty-first-century glacier mass change in the Himalayas. *Nature* 488(7412), 495-498.

Kirkbride, M.P. 2000. Ice-marginal geomorphology and Holocene expansion of debris-covered Tasman Glacier, New Zealand. *Debris-covered Glaciers: Proceedings of an international Workshop held at the University of Washington in Seattle, Washington, USA* 264: 211–218.

Kirkbride, M.P., Deline, P., 2013. The formation of supraglacial debris covers by primary dispersal from transverse englacial debris bands. *Earth Surface Processes and Landforms* 38, 1779–1792. doi:10.1002/esp.3416

Lenaerts, J. T. M., van den Broeke, M. R., van Wessem, J. M., van de Berg, W. J., van Meijgaard, E., van Ulft, L. H., Schaefer, M., 2014. Extreme precipitation and climate gradients in Patagonia revealed by high-resolution regional atmospheric climate modelling. *Journal of Climate*, 27, 4607–4621.

Loriaux, T., Casassa, G., 2013. Evolution of glacial lakes from the Northern Patagonia Icefield and terrestrial water storage in a sea-level rise context, *Global and Planetary Change*, 102, 33-40.

Marzeion, B., Cogley, J.G., Richter, K., Parkes, D. 2014 , Attribution of global glacier mass loss to anthropogenic and natural causes , *Science* , 345 , 919-921 , doi: 10.1126/science.1254702

Mattson LE. 2000. The influence of a debris cover on the mid-summer discharge of Dome Glacier, Canadian Rocky Mountains. *Debris-covered Glaciers: Proceedings of an international Workshop held at the University of Washington in Seattle, Washington, USA* 264: 25–34.

Mernild, S., Pelto, M., Malmros, J., Yde, J. Knudsen, N., Hanna, E. 2013. Identification of snow ablation rate, ELA, AAR and net mass balance using transient snowline variations on two Arctic glaciers, *Journal of Glaciology*, 59, 649–659, doi:10.3189/2013JoG12J221.

Mihalcea, C., Mayer, C., Diolaiuti, G., D'Agata, C., Smiraglia, C., Lambrecht, A., Vuillermoz, E., Tartari, G. 2008. Spatial distribution of debris thickness and melting from remote-sensing and meteorological data, at debris-covered Baltoro glacier, Karakoram, Pakistan. *Annals of Glaciology* 48: 49–57. DOI: 10.3189/172756408784700680

Mouginot, J., Rignot, E. 2015. Ice motion of the Patagonian Icefields of South America: 1984-2014. *Geophysical Research Letters* 42 (5), 1441–1449. doi: 10.1002/2014GL062661

Nakawo M, Rana B. 1999. Estimate of ablation rate of glacier ice under a supraglacial debris layer. *Geografiska Annaler: Series A,* 81, 695–701. DOI: 10.1111/1468-0459.00097

Nakawo, M., Takahashi, S. 1982. A simplified model for estimating glacier ablation under a debris layer, IAHS Publ. 138, 137–145.

Østrem, G., 1959. Ice melting under a thin layer of moraine, and the existence of ice cores in moraine ridges. *Geografiska Annaler* 41, 228–230.

Østrem G (1975) ERTS data in glaciology—an effort to monitor glacier mass balance from satellite imagery. *Journal of Glaciology* 16, 403–415.

Paul, F., Huggel, C., Kääb, A. 2004. Combining satellite multispectral image data and a digital elevation model for mapping debris-covered glaciers. *Remote Sensing of Environment* 89, 510-518.

Pellicciotti, F., Stephan, C., Miles, E., Herreid, S., Immerzeel, W.W., Bolch, T. 2015. Mass-

balance changes of the debris-covered glaciers in the Langtang Himal, Nepal, from 1974 to 1999. *Journal of Glaciology*, 61, 1–14. doi:10.3189/2015JoG13J237

Pelto, M. 2000. Mass balance of adjacent debris-covered and clean glacier ice in the North Cascades, Washington, IAHS Publ., 264, 35–42,.

Pelto, M., Capps, D., Clague, J. J., Pelto, B. 2013. Rising ELA and expanding proglacial lakes indicate impending rapid retreat of Brady Glacier, Alaska. *Hydrological Processes* 27, 3075–3082. doi: 10.1002/hyp.9913

Rasmussen, L. Conway, H., Raymond, C. 2007. Influence of upper air conditions on the Patagonia Icefields. *Global and Planetary Change*, 59, 203–216.

Reznichenko, N.V., Davies, T.R.H., Alexander, D.J. 2011. Effects of rock avalanches on glacier behaviour and moraine formation. *Geomorphology*, 132, 327-338.

Richardson, S.D. and Reynolds, J.M. 2000. An overview of glacial hazards in the Himalayas. *Quaternary International*, 65-66, 31-47.

Rignot, E., Rivera, A., Casassa, G., 2003. Contribution of the Patagonia Icefields of South America to sea level rise. *Science*, 302, 434–437.

Rivera, A., Benham, T., Casassa, G., Bamber, J., Dowdeswell, J.A. 2007. Ice elevation and areal changes of glaciers from the Northern Patagonia Icefield, Chile. *Global and Planetary Change*, 59, 126–137.

Rosenblüth, B. Casassa, G., Fuenzalida H. 1995. Recent climatic changes in western Patagonia *Bulletin of Glaciological Research*, 13, 127–132.

Rowan, A.V., Quincey, D.J., Egholm, D.L., Glasser, N.F. 2015. Modelling the feedbacks between mass balance, ice flow and debris transport to predict the response to climate change of debris-covered glaciers in the Himalaya. *Earth and Planetary Science Letters,* 430, 427-438. doi:10.1016/j.epsl.2015.09.004

Scherler, D., Bookhagen, B., Strecker, M.R., 2011. Spatially variable response of Himalayan glaciers to climate change affected by debris cover. *Nature Geoscience* 4, 156–159. doi:10.1038/ngeo1068

SERNAGEOMIN 2003. *Mapa Geológico de Chile: versión digital, escala 1:1,000,000*. Servicio Nacional de Geología y Minería, Santiago, Chile.

Shroder, J. F., Bishop, M. P., Copland, L., Sloan, V. F. 2000. Debris-covered Glaciers and Rock Glaciers in the Nanga Parbat Himalaya, Pakistan. *Geografiska Annaler* 82A: 17–31.

Shugar, D. H., Rabus, B. T., Clague, J. J., Capps, D. M. 2012. The response of Black Rapids Glacier, Alaska, to the Denali earthquake rock avalanches. *Journal of Geophysical Research-Earth Surface,* 117.

Takeuchi, Y., Kayastha, R. B., Nakawo, M. 2000. Characteristics of ablation and heat balance in debris-free and debris-covered areas on Khumbu Glacier, Nepal Himalayas, IAHS Publ., 264, 53–61.

White, A., Copland, L. 2015. Decadal-Scale Variations in Glacier Area Changes across the Southern Patagonian Icefield since the 1970s. *Arctic, Antarctic, and Alpine Research* 47(1), 147-167.

Willis, M.J., Melkonian, A.K., Pritchard, M.E., Ramage, J.M. 2012. Ice loss rates at the Northern Patagonian Icefield derived using a decade of satellite remote sensing. *Remote Sensing of Environment*, 117, 184-198.

Winchester, V., Harrison, S. 1996. Recent oscillations of the San Quintin and San Rafael glaciers, Patagonian Chile. *Geografiska Annaler* 78A, (1): 35-49.

Winchester, V., Harrison, S. 1997. Estimate of ice surface velocity over a four year period on the Arenales Glacier, North Patagonian Icefield, Chile. *Journal of Glaciology,* 43, 144. 370-372.

List of Figures

Fig. 1. Composite Landsat-7 image (11/03/2001) of the North Patagonian Icefield (NPI) in Southern South America indicating the main glacier catchments and outlet glaciers.

Fig. 2. (A) Number of glaciers and total glacierized area in different glacier size classes. (B) Histogram of proglacial lake area. (C) Scatterplot showing original glacier area in 1987 against glacier area change (km^2). (D) Scatterplot showing glacier area change (km^2) against glacier debris cover in 2015. Larger glaciers tend to have more debris-covered area (km^2) and tend to have lost most glacier area (km^2).

Fig. 3.(A) Glacier extent in 1987, 2001, and 2015. Blue indicates glaciers west of the ice divide; red indicates glaciers east of the ice divide. Blue circles are percentage debris cover. (B)As (A), but 2015 glacier extent colored according to annual rate of recession (% a^{-1}) from 2001 to2015. (C) As (A), but 2015 glacier extent colored according to maximum rate of velocity (m/y) from Mouginot and Rignot (2015).

Fig. 4. Glaciar Grosse on the northern side of the NPI, a debris-covered glacier where the entire ablation area is debris-covered in 2015 {21st January 2015} Note also the large proglacial lake (image: Landsat 8 OLI-TIRS LC82320922015021LGN00 from 21st January 2015)

Fig. 5. (A) Lake areas for individual glaciers of the NPI in 1987, 2001, and 2015. Note the rapid expansion of proglacial lakes at Glaciar San Quintin, which has grown in area from ~18 km^2 in 1987 to ~54 km^2 in 2015. (B) Lake area changes for individual glaciers of the NPI for the periods 1987-2001, 2001-2015 and the entire period 1987-2015. Note that expansion of the proglacial lake at Glaciar San Quintin also dominates the change in lake area over this time period. (C) Percentage change in lake area through time.

Fig. 6. Detail of changes at the snout of Glaciar Fiero between 2001 and 2015. The white line (arrowed) indicates the position of the glacier terminus in 2001 in both cases. Note the expansion of the large proglacial lake at Glaciar Fiero (arrowed) and the changes in surface debris cover. A new glacial lake has also formed at the adjacent glacier (arrowed) in the 14 years between 1987 and 2015.

Fig. 7. (A) The extent of the debris-covered area on the largest individual outlet glaciers of the NPI in 1987, 2001, and 2015. (B) Debris-cover change by glacier for the periods 1987-

2001, 2001-2015, and the entire period from 1987 to2015. Note that several large glaciers (e.g. Glaciar San Rafael, Glaciar Gualas, Glaciar San Quintin, and Glaciar Steffen) actually lost large areas of debris cover between 1987 and 2001 before debris cover then increased between 2001 and 2015.

Fig. 8. Detail of debris features that have appeared on glacier surfaces between 2001 and 2015. (A) Large rockfall deposited on the surface of Glaciar Grosse. (B) Large lobate rockfall deposited on the surface of Glaciar Pissis. Note also the recession of the ice front over this time. (C) Large rockfall deposited on the surface of Glaciar Leones. Note the large run out zone and how the rockfall obscures the existing medial moraines on the glacier surface.

Fig. 9. Detail of changes in ice-surface debris and transport through time (1987-2001-2015). (A) New patch of debris (arrowed) appeared on the surface of Glaciar Colonia in 1987 and was transported down-ice between 2001 and 2015. (B) Immediately below the icefall on Glaciar Pared, a rockfall deposited on the ice surface (arrowed) was transported rapidly down-ice to merge with existing supraglacial debris. (C) Closer to the terminus of Glaciar Pared Norte, a second rockfall (arrowed) was also transported rapidly down-ice along the lateral margin in the period 1987-2001-2015.

Fig. 10. Oblique aerial photograph of Leones Glacier showing recent large rockfall on the glacier surface (orange arrows). This is the same rockfall as Fig. 8C. The red arrow indicates the terminus of North Leones Glacier (photograph: Jill Pelto, 13th March 2015).

Fig. 11. (A) Area of debris-covered ice in 100-m elevation bands. (B) Change in area of debris-covered ice in 100-m elevation bands between 1987 and 2015. Note the loss of ~19 km^2 below an elevation of 100 m caused by the reduction of glacier ice at this low elevation.

Fig. 12. Example of the interplay between changes in glacier area, debris cover and lake area for Glaciar Steffen (A-C), Glaciar San Quintin (D-F), and Glaciar Grosse (G-I).

Table 1: Data sources used in this study

Platform/Sensor/Image ID	Date acquired (d/m/y)	Comments e.g. clouds etc
Landsat 8 OLI-TIRS (LC82320922015021LGN00)	21/01/2015	Northern section
Landsat 8 OLI-TIRS (LC82320932015021LGN00)	21/01/2015	Southern section02/11/2014 was also used because of cloud cover on Glaciar San Quintin
Landsat 8 OLI-TIRS (LC82320932014306LGN00)	02/11/2014	Southern section
Landsat 7 ETM (LE72320922001070EDC00)	11/03/2001	Northern section
Landsat 7 ETM (LE72320932001070EDC00)	11/03/2001	Southern section
Landsat 5 MSS (LM52320921987040AAA04)	09/02/1987	Northern section
Landsat 5 MSS (LM52320931987040AAA03)	09/02/1987	Southern section

Table 2: Time taken between different time intervals in days and years.

Time period	Number of days	Number of years
2001-2015	5064	13.9
2001-2014[a]	4984	13.7
1987-2001	5144	14.1
1987-2015	10208	28.0
1987-2014[a]	10128	27.8

[a]San Quintin only.

Table 3. Glacier area and number of glaciers in the NPI in 2015.

Glacier area	Total area (km^2)	Number of glaciers
0 to 1 km^2	0.00	0
1 to 10 km^2	76.6	14
10 to 50 km^2	305.9	14
50 to 100 km^2	417.4	6
100 to 500 km^2	1596.8	7
> 500 km^2	1493.9	2
Total	*3890.6*	*43*

Table 4. Regression analysis of glacier characteristics in 2015.

X variable	Y variable	Pearson's	R^2
Mean Slope (°)	Max Velocity (m/y)	-0.36	0.13
Max Velocity (m/y)	% Debris cover	0.08	0.07
Glacier Area (km^2)	Max Velocity (m/y)	0.41	0.17
Mean Slope (°)	Lake area (km^2)	-0.45	0.21
Glacier Area (km^2)	Lake area (km^2)	0.75	0.56[a]
Zmax (m asl)	Max Velocity (m/y)	0.39	0.15
Glacier Area (km^2)	Debris cover (km^2)	0.74	0.55[a]
Glacier Area (km^2)	Mean Slope	-0.62	0.39
Mean Slope (°)	Debris cover (km^2)	-0.54	0.29
Mean Slope (°)	% Debris cover	-0.11	0.01
Glacier Area (km^2)	% Debris cover	-0.08	0.01
Velocity (m/y)	Debris cover (km^2)	0.06	0.00

[a]Significant values.

Table 5. Change in glacierized area (excluding nunataks) east and west of the ice divide

	Total	East of ice divide	West of ice divide
n of glaciers (2015)	43	26	17
Glacierized area 2015 (km^2)	3890.5	1037.2	2853.3
Glacierized area 2001 (km^2)	4035.1	1093.7	2941.4
Glacierized area 1987 (km^2)	4133.1	1098. 5	3034.6
Area change 1987 to 2001 (km^2)	-97.9	-4.8	-93.2
Area change 2001 to 2015 (km^2)	-144.6	-56.5	-88.1
% change 2001 to 2015	-3.6	-5.2	-3.0
% change 1987 to 2001	-2.4	-0.4	-3.1
% change per annum (% a^{-1}) 2001-2015	-0.3	-0.4	-0.2
% change per annum (% a-1) 1987-2001	-0.2	-0.03	-0.2

Table 6. Change in proglacial lake extent, 1987-2015

	Total	East of ice divide	West of ice divide
Proglacial lake extent (km^2) 2015	197.7	82.9	114.8
Proglacial lake extent (km^2) 2001	150.3	73.4	76.9
Proglacial lake extent (km^2) 1987	111.9	66.3	45.5
Lake area change 1987 to 2001 (km^2)	38.5	7.1	31.4
Lake area change 2001 to 2015 (km^2)	47.4	9.5	37.9
% change 2001 to 2015	31.5	12.9	49.2
% change 1987 to 2001	34.4	10.7	69.0

Table 7. Number, area, and proportional area of debris-covered glaciers in each region and time period

	Year	Total	East of ice divide	West of ice divide
Number of debris-covered glaciers	**2015**	32	19	13
	2001	31	19	12
	1987	24	13	11
Total debris-covered area (km^2)	**2015**	306.6	157.1	149.5
	2001	228.6	135.4	93.2
	1987	168.5	119.2	49.3
Total proportion of debris-covered area (%)	**2015**	7.9	15.2	5.2
	2001	5.7	12.4	3.2
	1987	4.1	10.9	1.6

Table 8. Relationship between debris cover and rates of recession

x variable	y variable	Pearsons	RSQ
Glacier area 1987	Rate of recession 1987-2015	0.08	0.01
% Debris cover 2015	Rate of recession 1987-2015	-0.15	0.02
Debris cover 2015 (km^2)	**Amount of change 1987-2015 (km^2)**	**-0.76**	**0.57**
Glacier slope	Rate of recession 1987-2015	0.05	0.00
Debris cover 2015 (km^2)	Rate of recession 1987-2015	0.04	0.00
Max velocity	Rate of recession 1987-2015	0.33	0.11
Glacier area 1987	**Amount of change 1987-2015 (km^2)**	**-0.89**	**0.78**
ZMAX	Rate of recession 1987-2015	0.09	0.01

Table 9: Transient snow line observations from Landsat images (2013-2016) indicating the highest observation for a given year on 11 glaciers of the NPI.

Glacier	87/2013[a]	50/2014[a]	85/2015[a]	72/2016[a]	Mean 2013-2016	1979/2003 (Barcaza et al., 2009)	Difference
Steffen	1200	1075	1025	1100	1100	1000	100
Acodado	1200	1075	1025	1110	1103		
HPN1	1075	1000	950	1075	1025	897	128
Benito	Cloud	1000	950	1050	1000	876	124
San Quintin	1050	Cloud	975	1050	1025	950	75
San Rafael	1100	1075	1000	1075	1063	900	163
Gulalas	1200	1225	1200	1250	1219	996	223
Soler	1450	1425	1475	1475	1456	1390	66
Nef	1350	1300	1325	1350	1331	1250	81
Colonia	1350	1325	1300	1350	1331	1270	61
Pared Nord	1075	1050	1075	1100	1075	1020	55
Mean	1225	1233	1193	1236	1214	1111	103

[a]Dates are displayed as Julian Day/Year. These new data are compared to the Barcaza et al. (2009) data in the final two columns.

Table 10: Summary statistics for the North Patagonian Icefield (NPI) in 1987, 2001, and 2015

Year	NPI area (km^2)	Debris area (km^2)	Lake area (km^2)	Modal debris elevation (m)
1987	4133.1	246.3	111.9	501-600
2001	4031.4	231.9	150.3	601-700
2015	3886.9	310.6	197.7	601-700

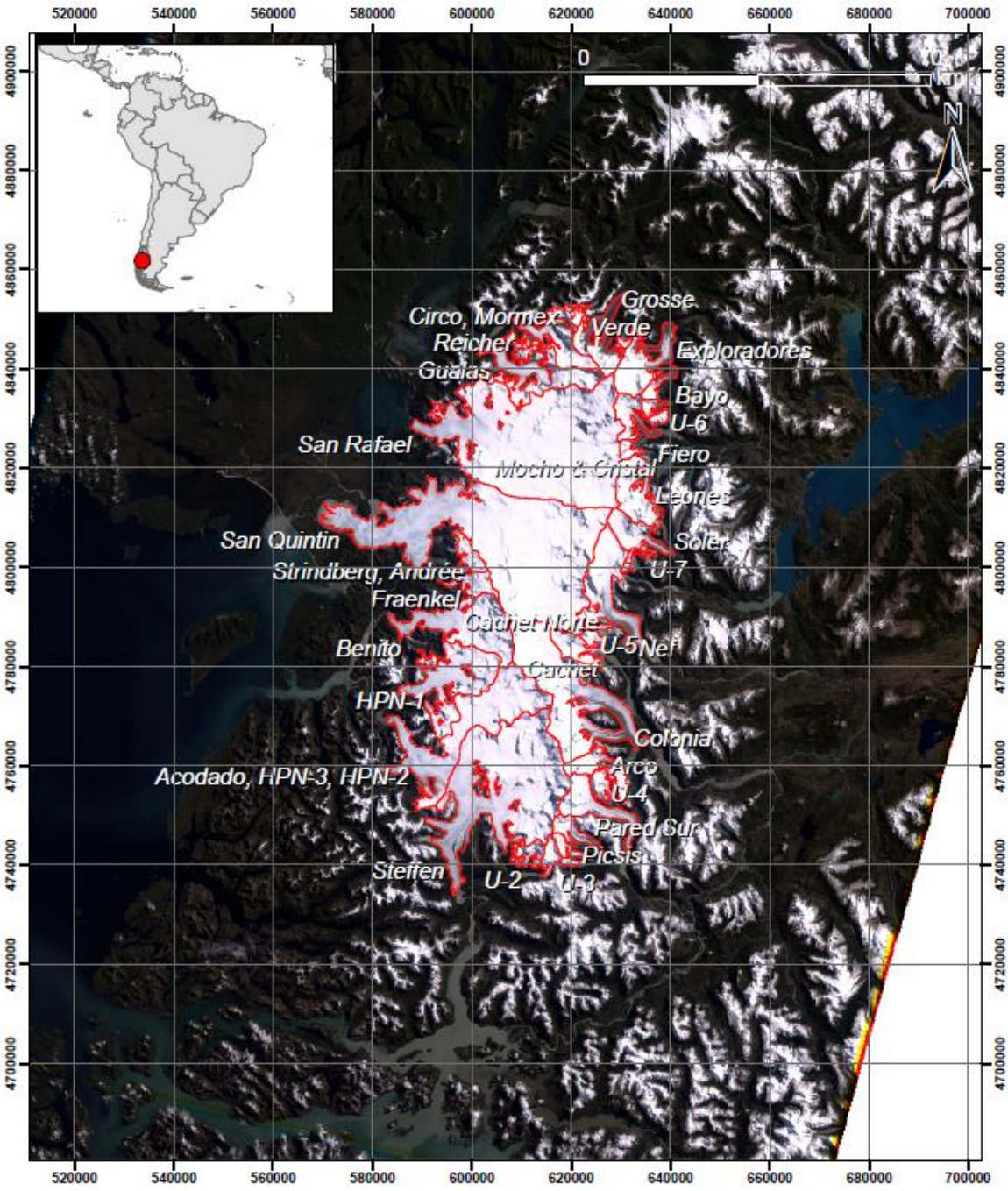

Figure 1

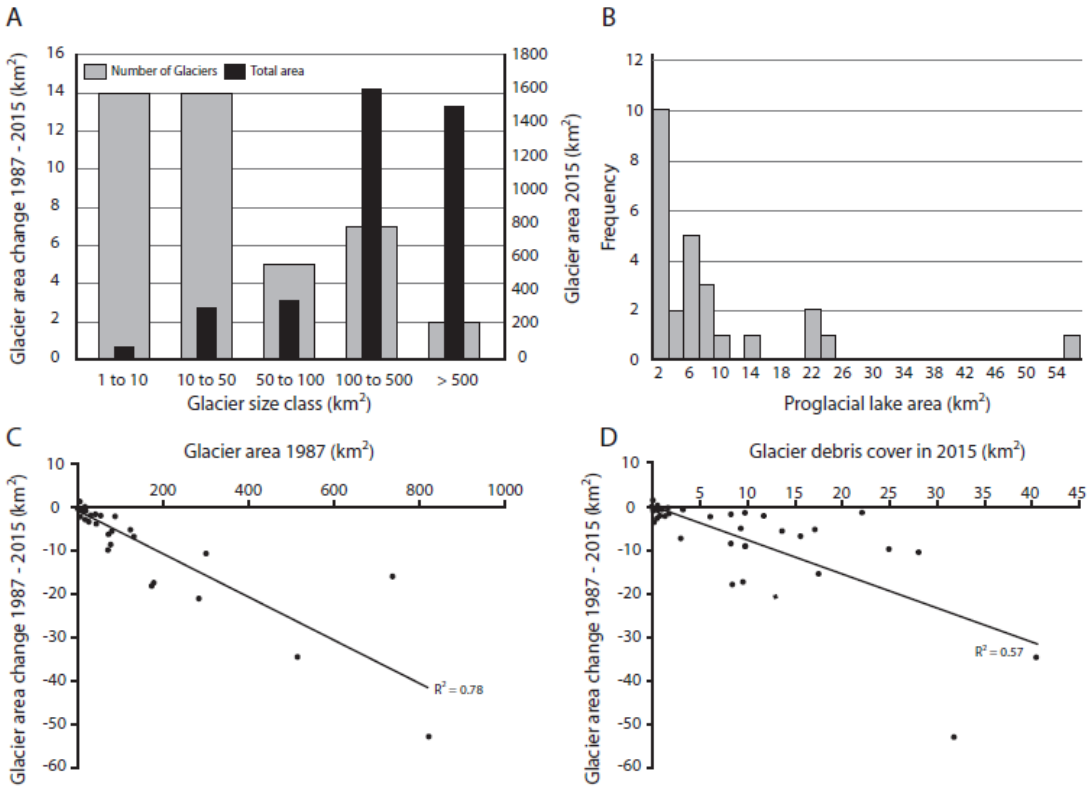

Figure 2

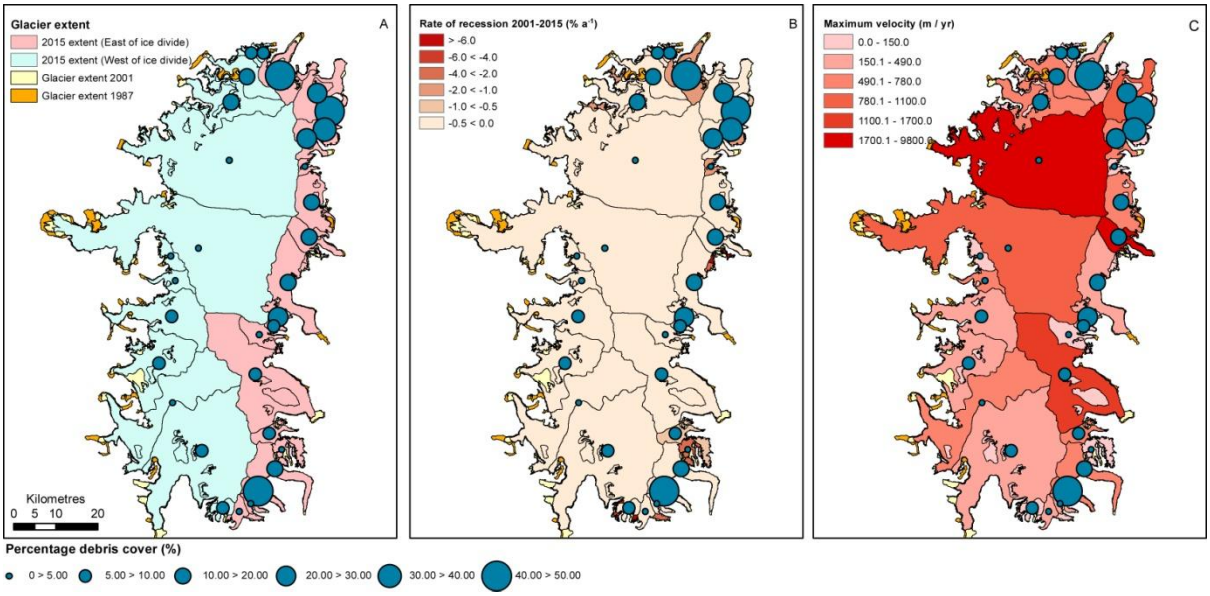

Figure 3

Figure 4

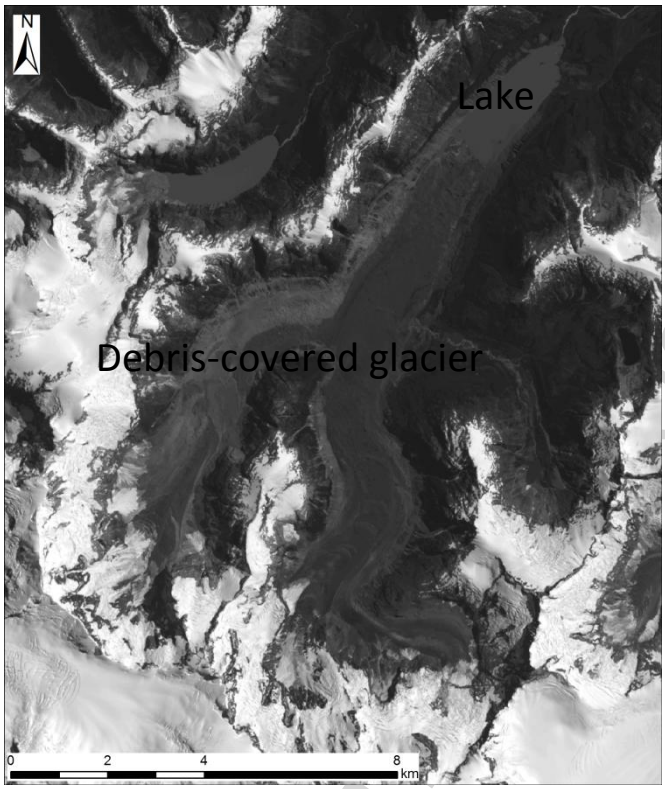

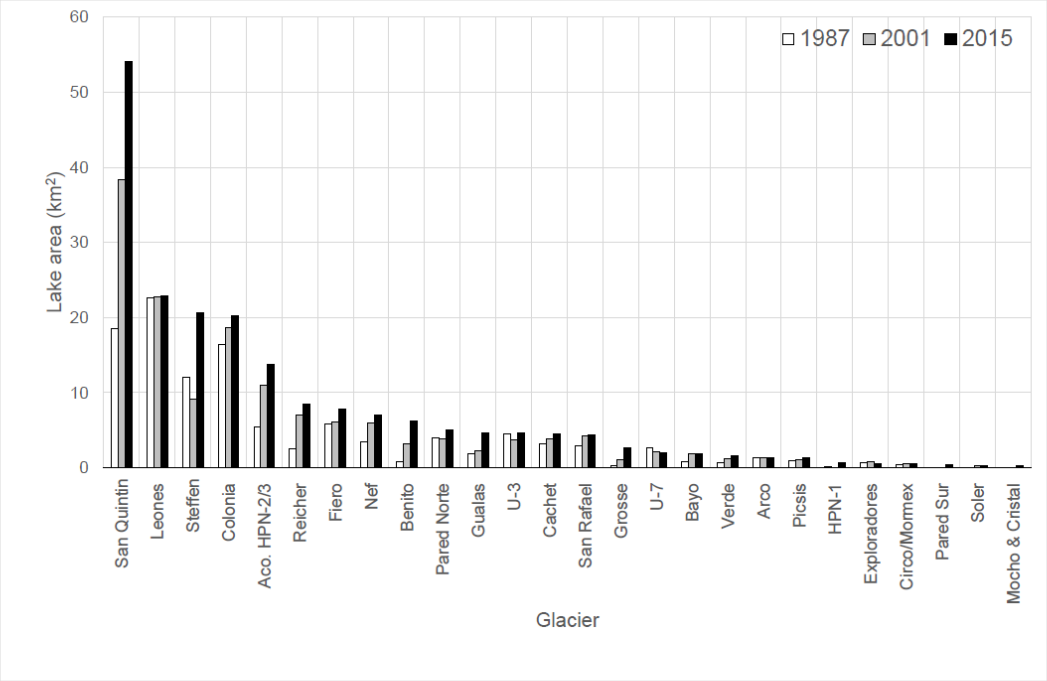

Figure 5A

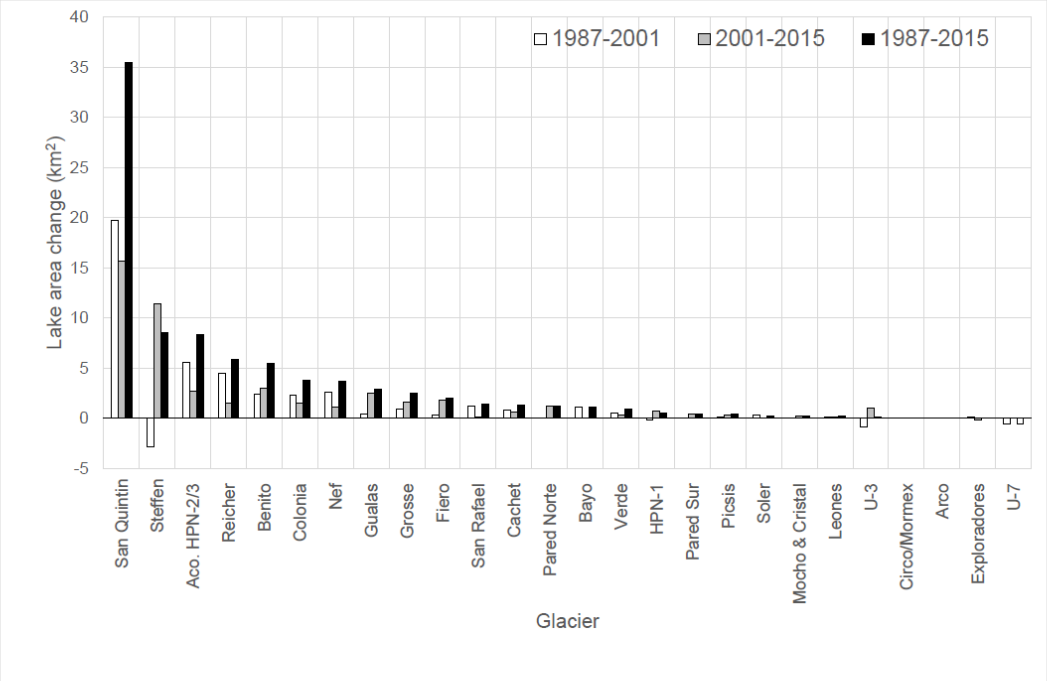

Figure 5B

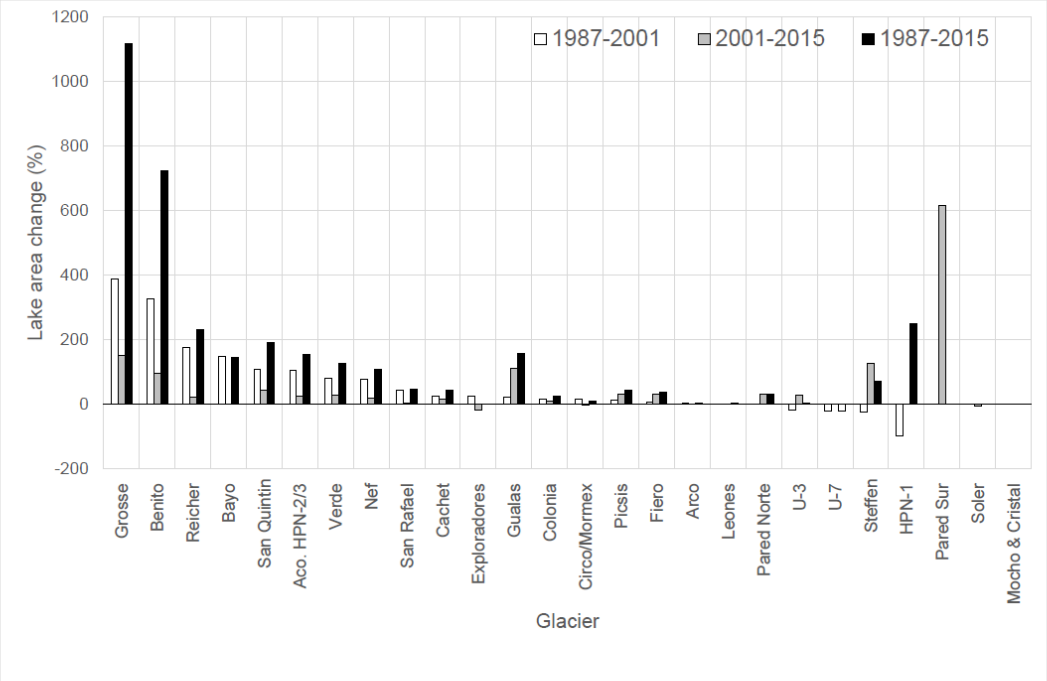

Figure 5C

11th March 2001

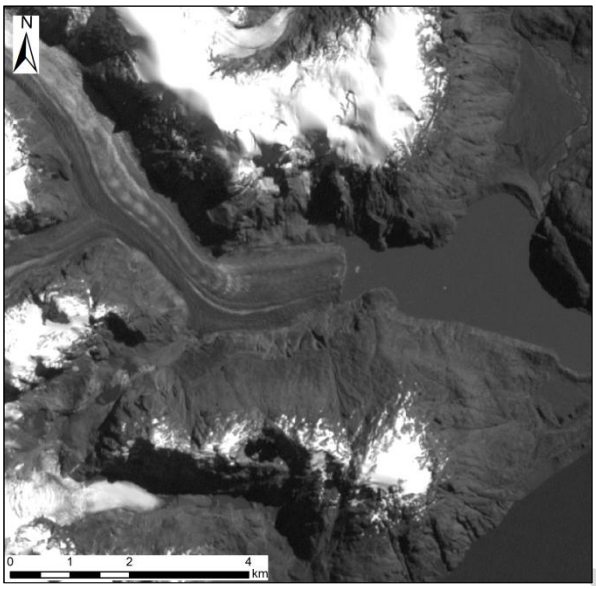

21st January 2015

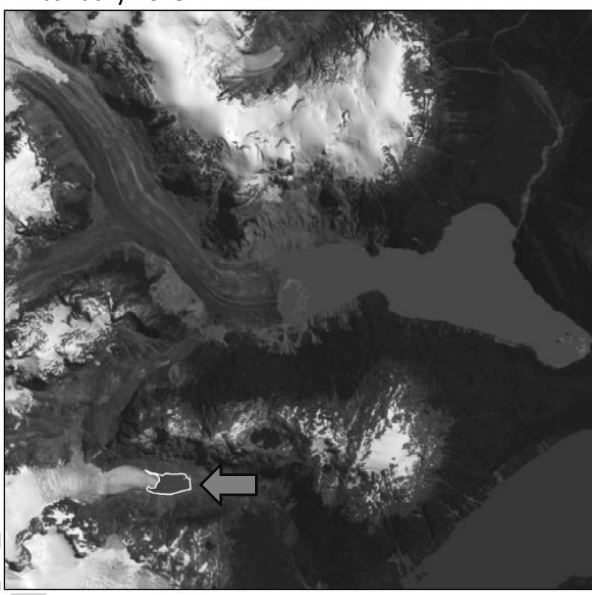

Figure 6

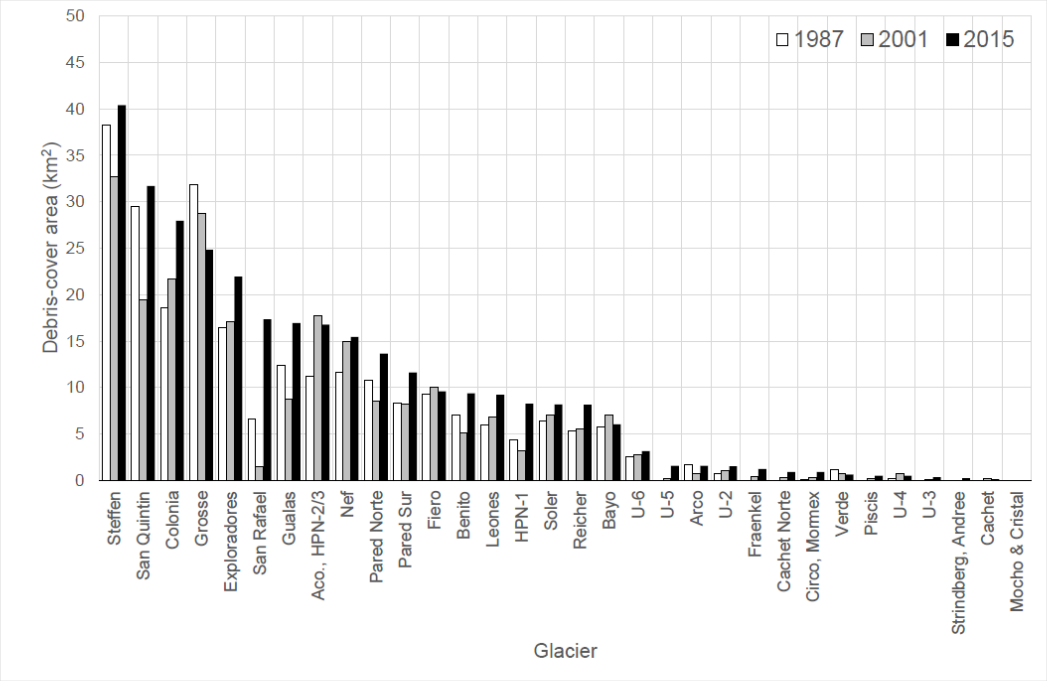

Figure 7A

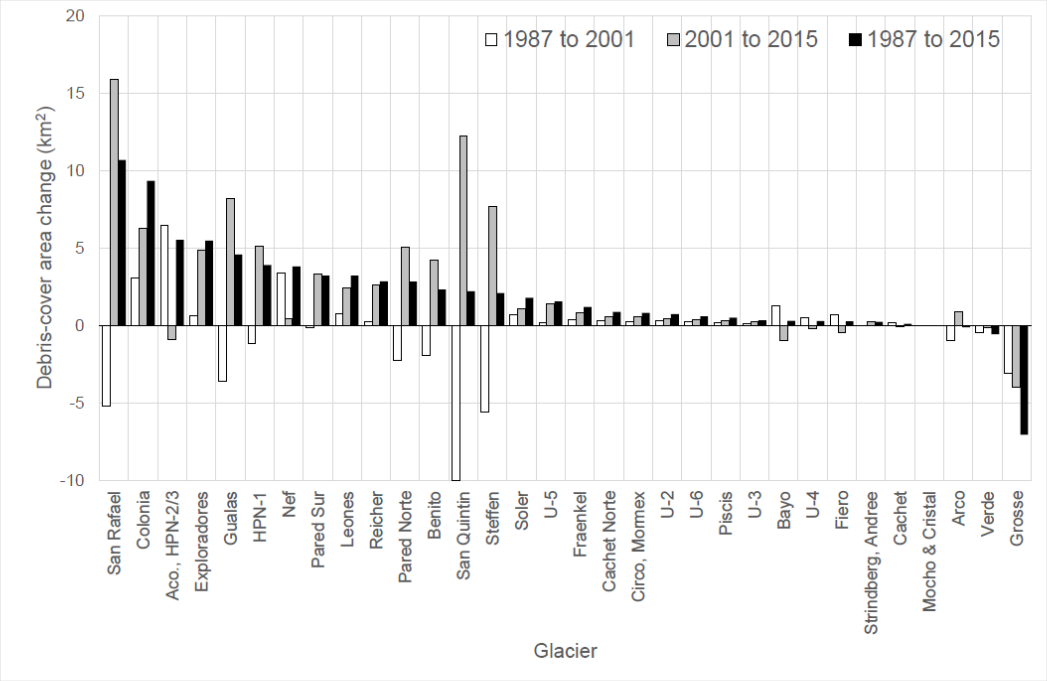

Figure 7B

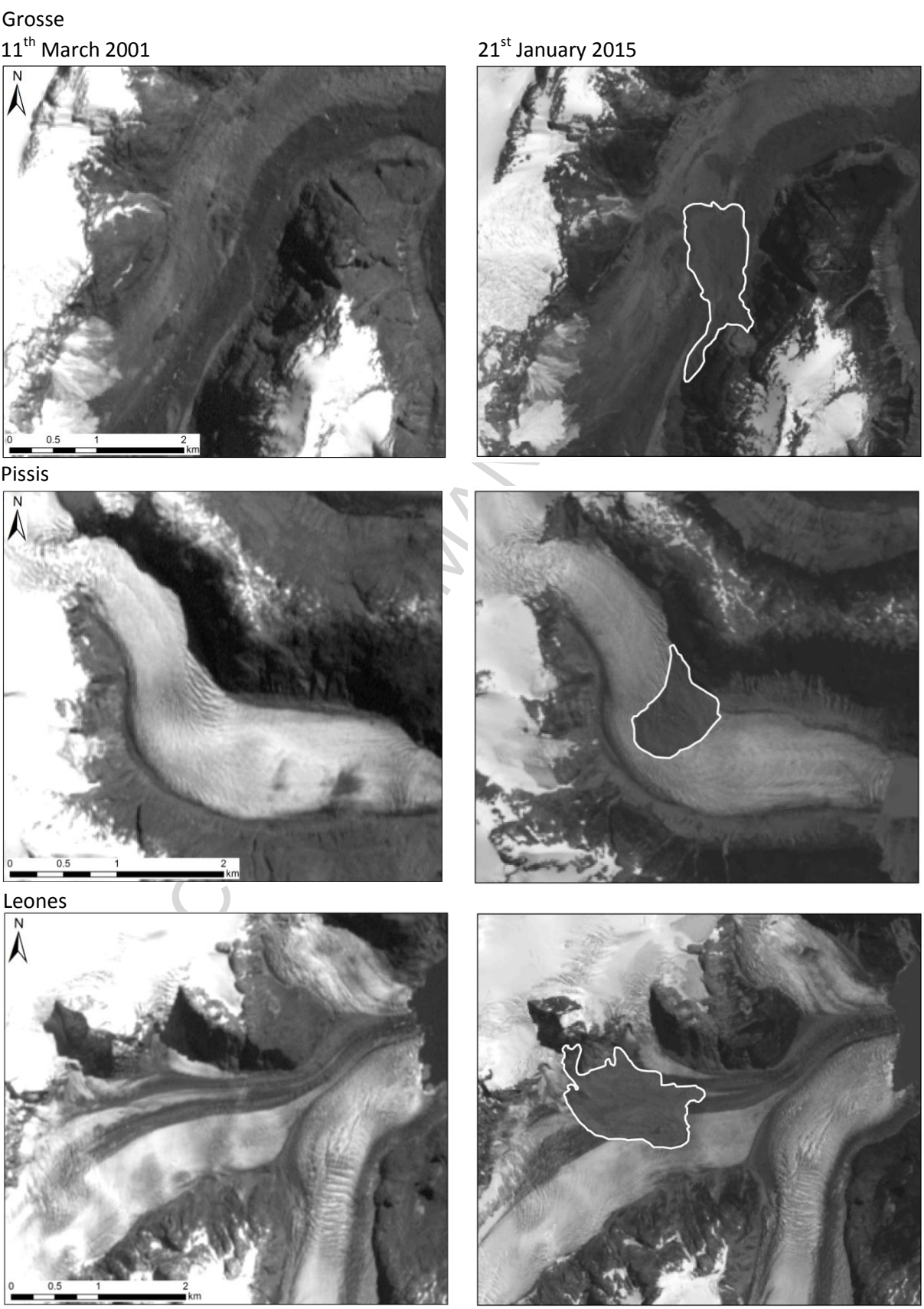

Figure 8

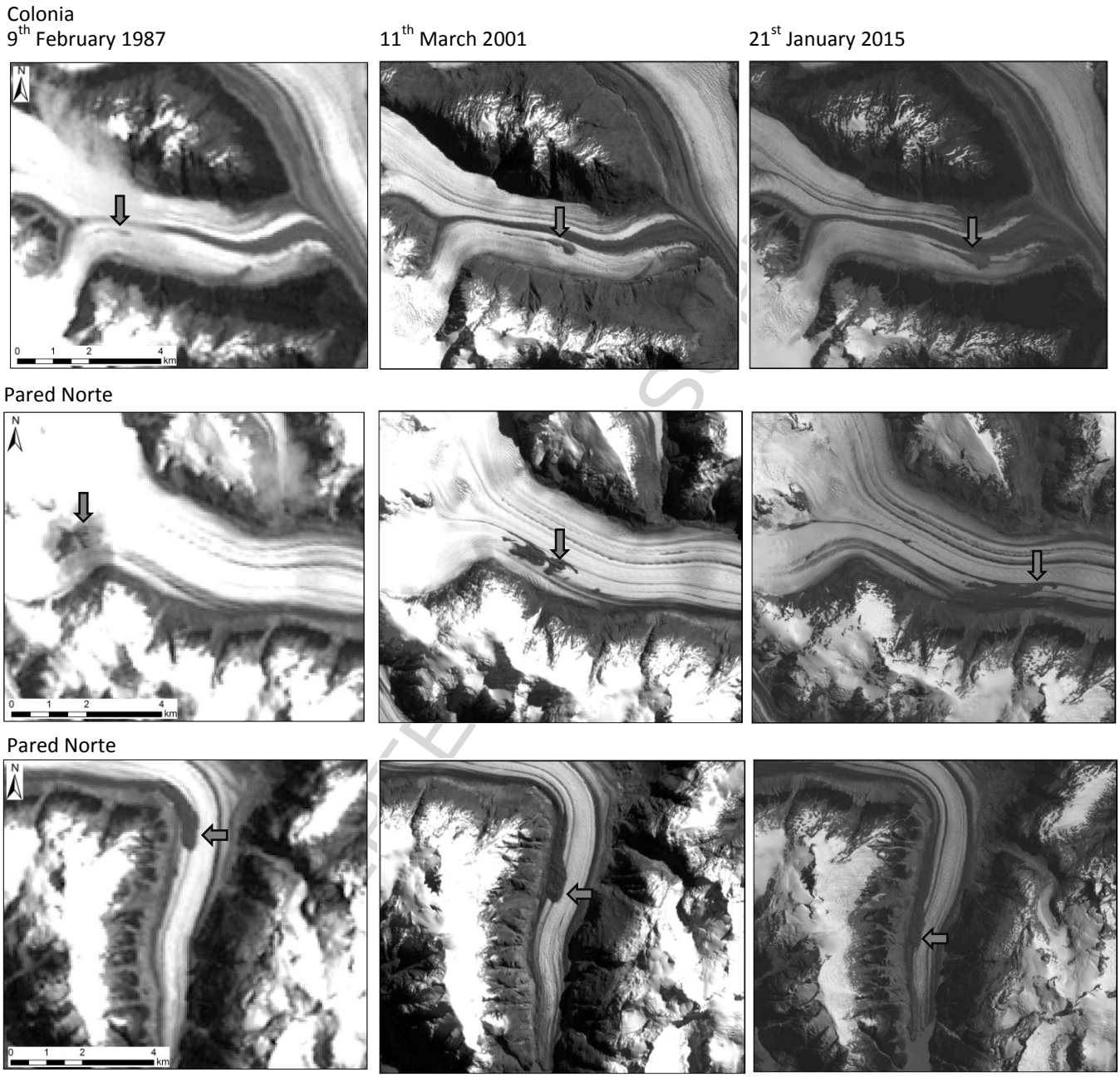

Figure 9

Figure 10

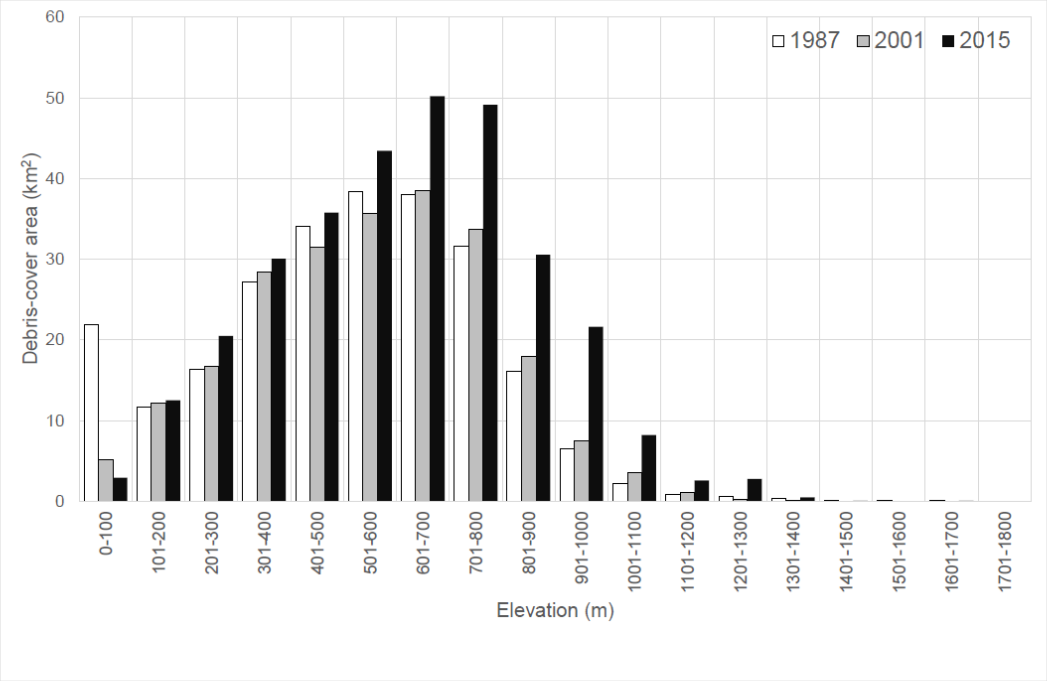

Figure 11A

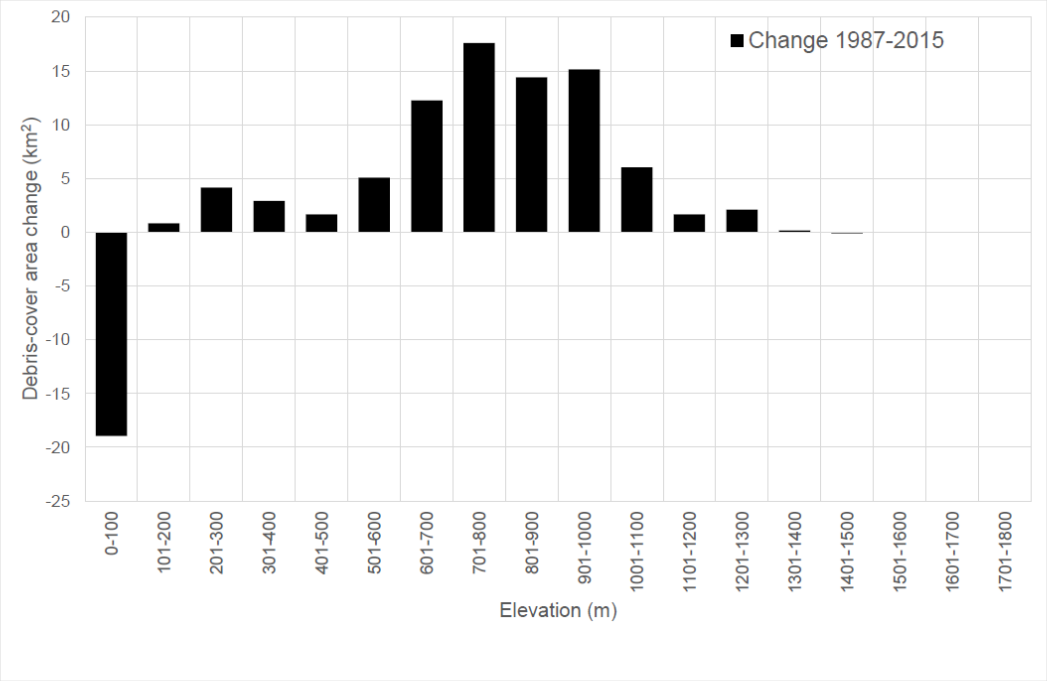

Figure 11B

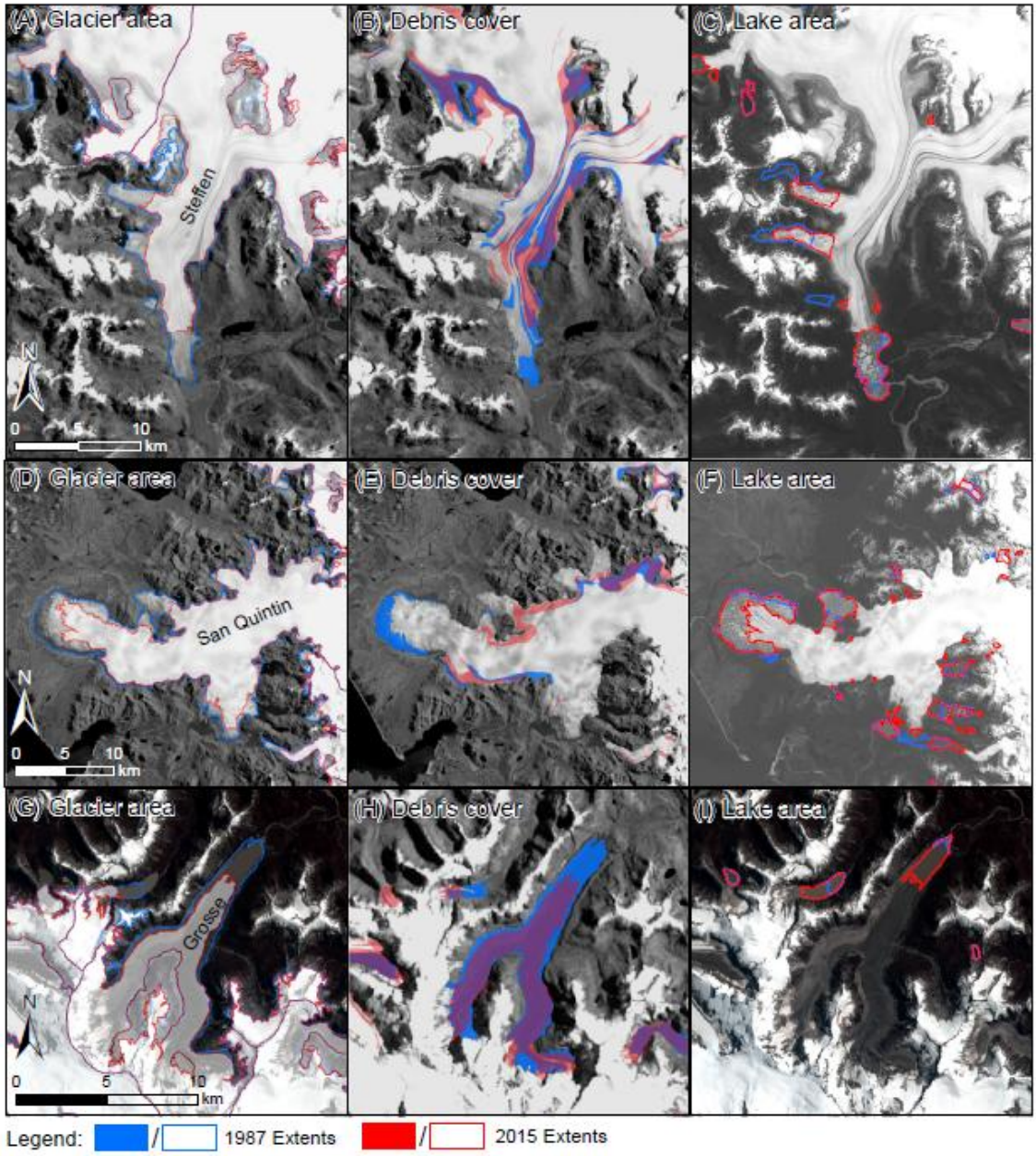

Figure 12